Supporting Information

Controllable Load Sharing for Soft Adhesive Interfaces on Three-Dimensional Surfaces

Sukho Song[1,2], Dirk-Michael Drotlef[1], Carmel Majidi[2], Metin Sitti[1,2,†]

[1] Physical Intelligence Department, Max Planck Institute for Intelligent Systems, 70569 Stuttgart, Germany

[2] Department of Mechanical Engineering & Robotics Institute, Carnegie Mellon University, Pittsburgh, PA 15213, USA

† Corresponding author email: sitti@is.mpg.de

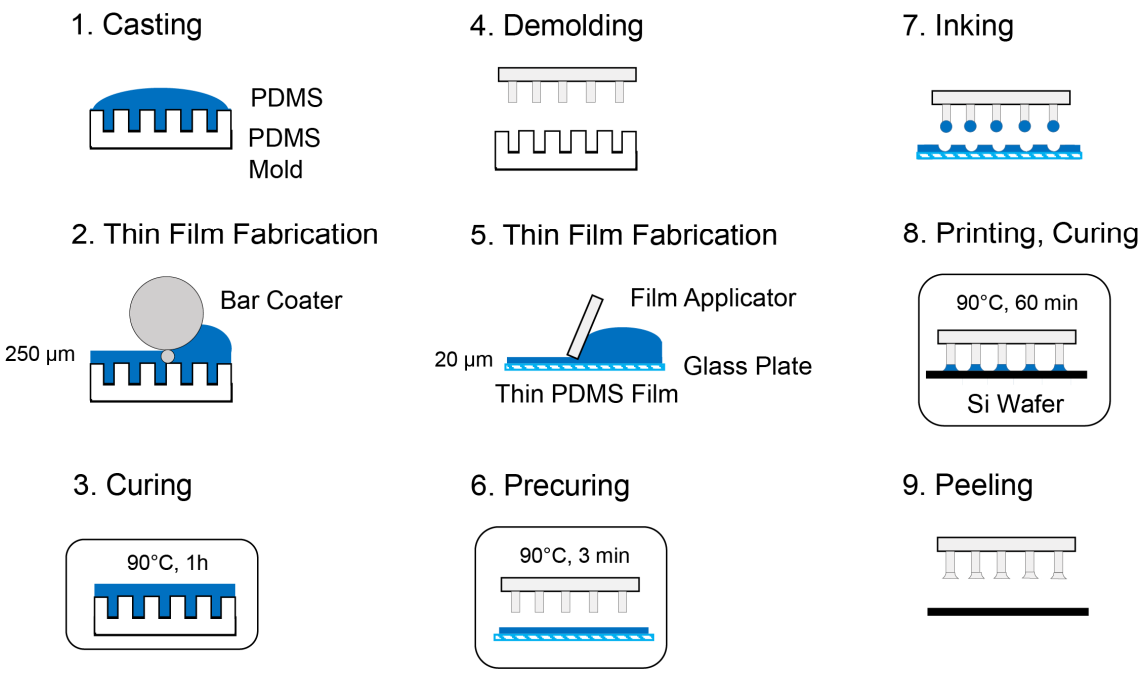

Fig. S1 Experimental procedure for fabricating the FAM. A schematic shows the individual steps of the fabrication process.

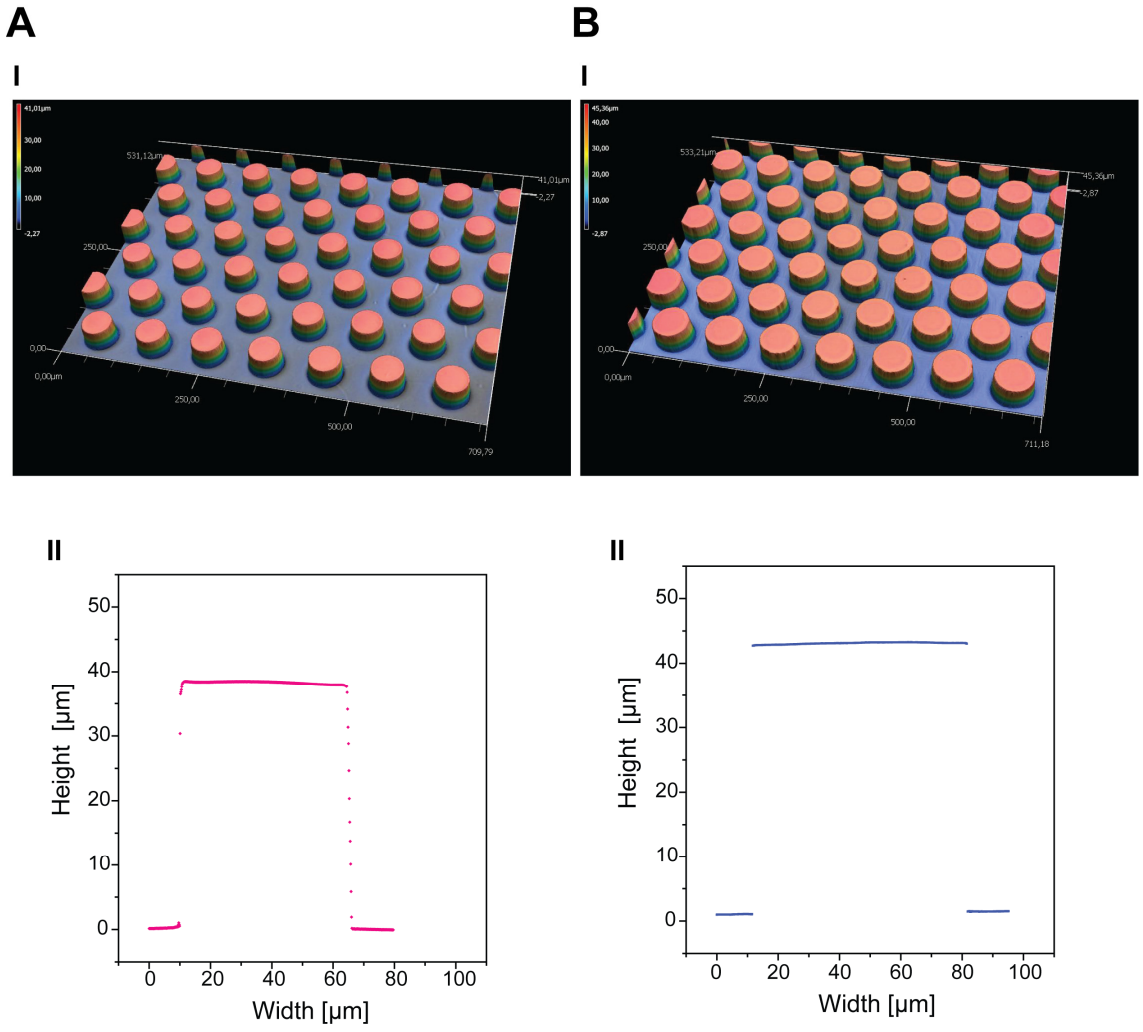

Fig. S2 3D scanned images of PDMS patterns and dimensions. (A) 3D image (I) and profile (II) of cylindrical PDMS patterns with 52-µm diameter, 48-µm spacing and 38-µm height. (B) 3D image (I) and profile (II) of mushroom shaped PDMS patterns with 69-µm diameter, 31-µm spacing and 42-µm height. Note that the pillar stems of the mushroom shaped patterns cannot be measured since they are covered by the overhanging tips.

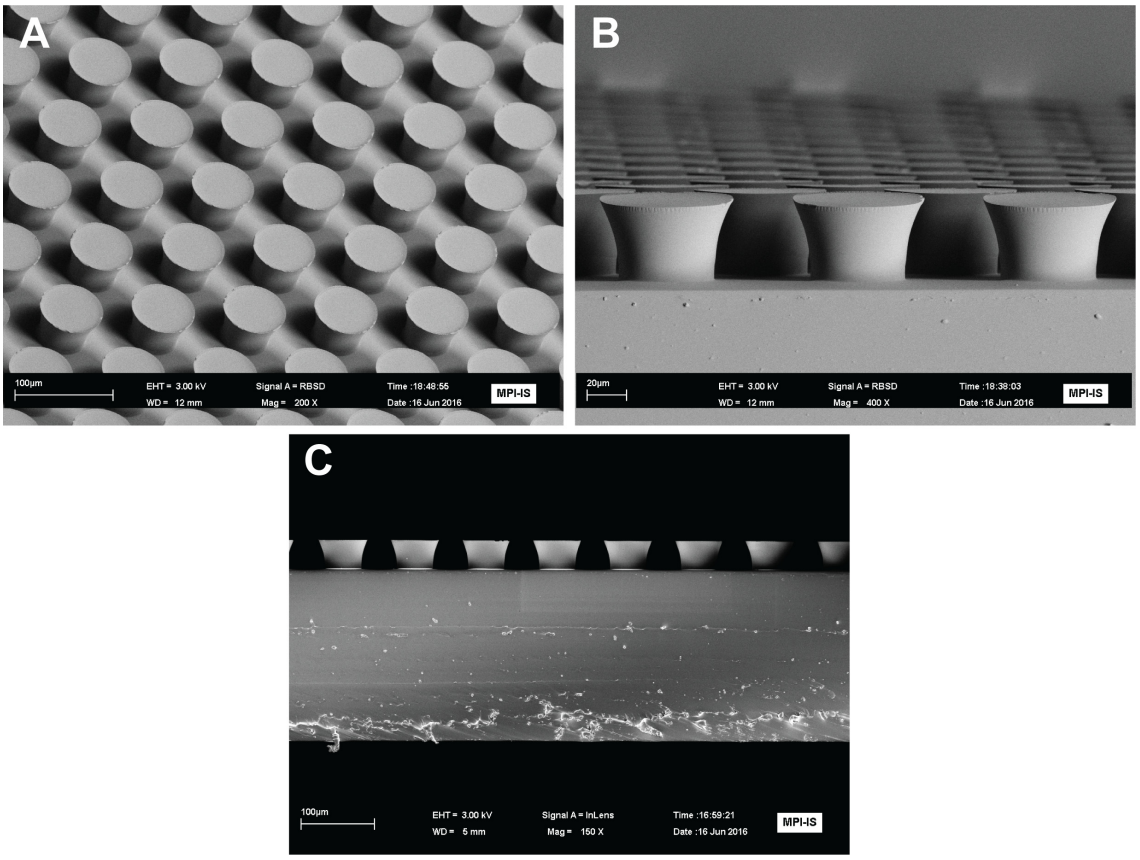

Fig. S3 SEM images of mushroom-shaped elastomer microfiber arrays on the FAM. Top (A) and side-view (B) of mushroom-shaped microfiber arrays with 69-µm in diameter, 31-µm in spacing, and 42-µm in height. (C) A side-view of the FAM supported by a thin backing layer with ca. 250-µm in thickness.

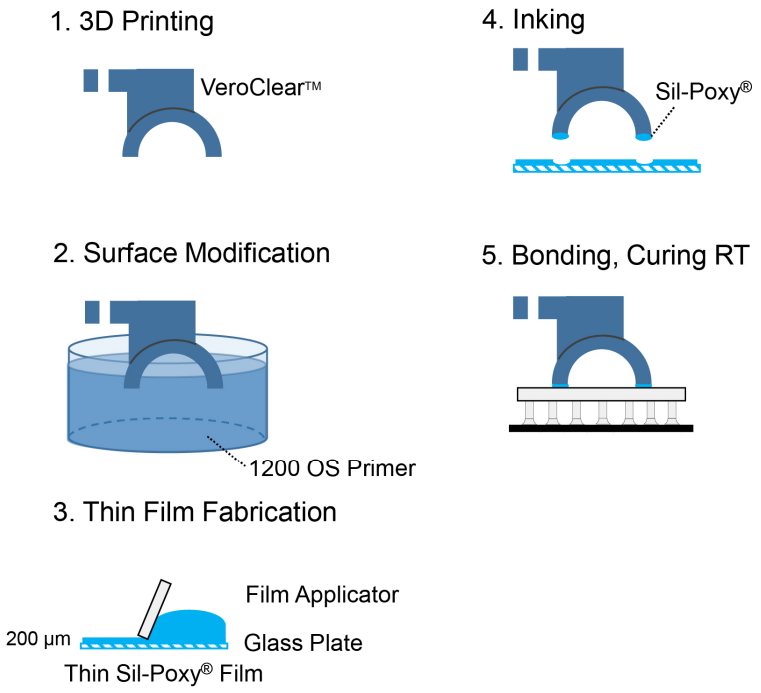

Fig. S4 Experimental procedure for fabricating the rigid adhesion system. A schematic shows the individual steps of the fabrication process for obtaining a rigid system with the FAM.

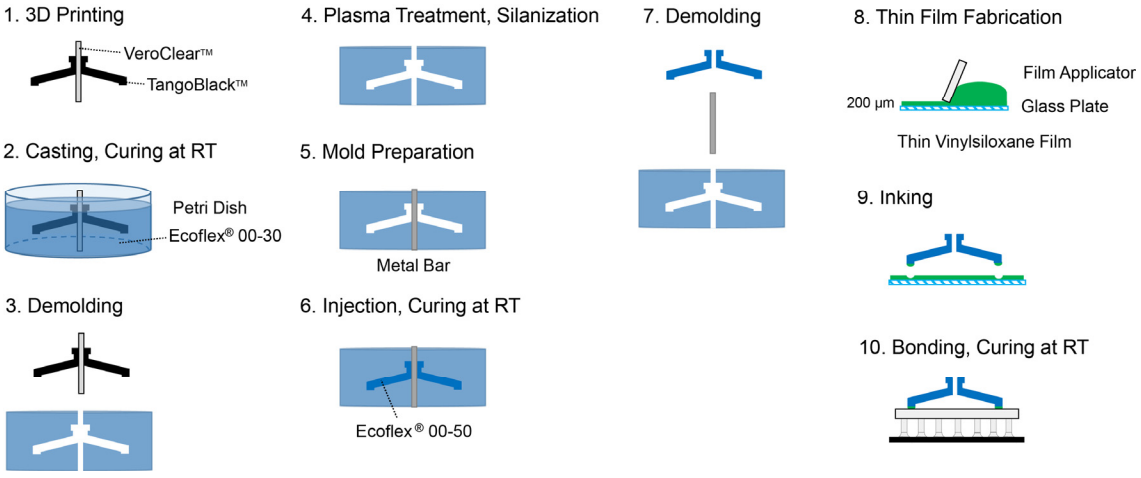

Fig. S5 Experimental procedure for fabricating the soft adhesion system. A schematic shows the individual steps of the fabrication process for obtaining a soft system with the FAM.

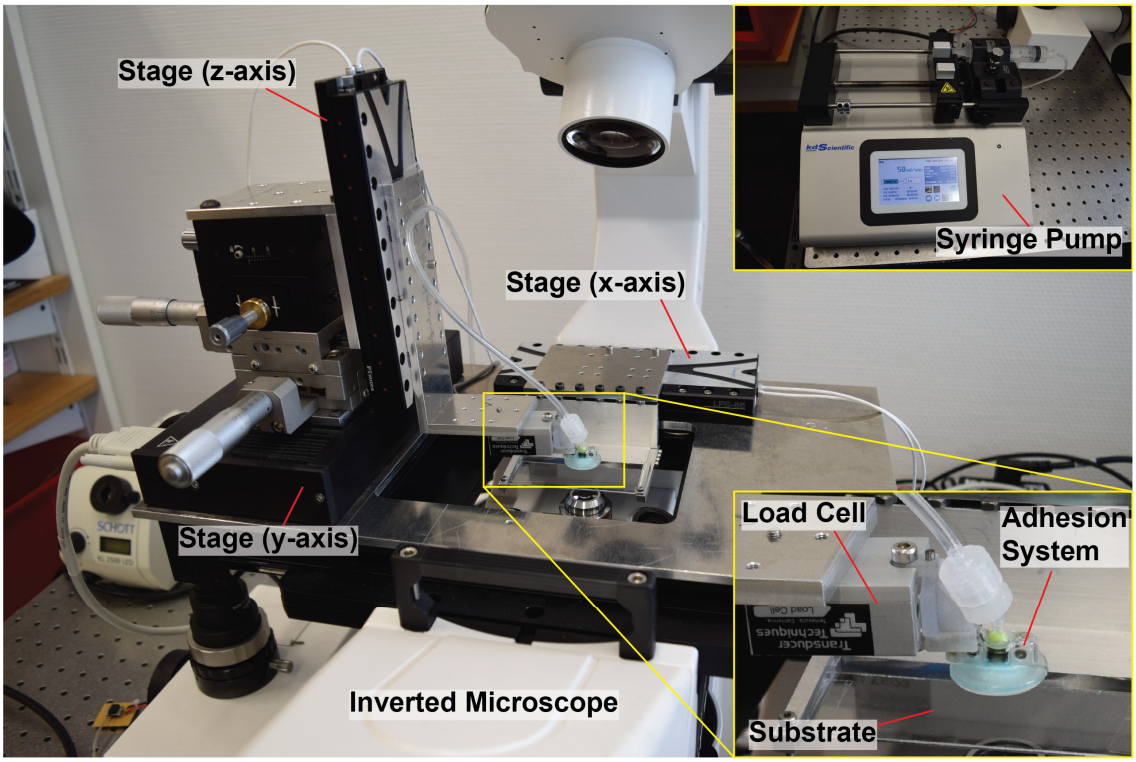

Fig. S6 Customized experimental setup for characterization of adhesion systems.

S1. Modeling Load Distribution among Microfibers

We perform a numerical calculation to obtain vertical stress (σ_{22}) within the FAM when pulling it up from a flat substrate under various differential pressures (ΔP_o). The FAM is simplified as an incompressible Hookean solid whose dimensions and boundary conditions are detailed in Fig. 3a. The analysis is further simplified by modeling the axisymmetric system in 2D and assuming plane strain conditions.

The elastic deformation is represented by a displacement field $\mathbf{u} = u_1(X_1,X_2)\mathbf{E}_1 + u_2(X_1,X_2)\mathbf{E}_2$, where the Cartesian coordinates X_1 and X_2 and Euclidean bases $\mathbf{E}_1$ and $\mathbf{E}_2$ correspond to the horizontal and vertical directions, respectively. According to the Hooke's law, stress in the $\mathbf{E}_1$–$\mathbf{E}_2$ plane has components (1)

$$\sigma_{11} = \frac{E_m}{1-\nu^2}\left(\frac{\partial u_1}{\partial X_1} + \nu\frac{\partial u_2}{\partial X_2}\right),\ \sigma_{22} = \frac{E_m}{1-\nu^2}\left(\nu\frac{\partial u_1}{\partial X_1} + \frac{\partial u_2}{\partial X_2}\right) \text{ and } \sigma_{12} = \sigma_{21} = \frac{E_m}{4(1+\nu)}\left(\frac{\partial u_1}{\partial X_2} + \frac{\partial u_2}{\partial X_1}\right). \quad [S1]$$

At static equilibrium, the stress tensor $\boldsymbol{\sigma}$ must satisfy the balance law $\nabla\cdot\sigma = 0$, where $\nabla =$ is the Lagrangian nabla operator. For 2D plane-strain elasticity, divergence-free stress implies the following form of the Navier-Lame equations:

$$\frac{\partial^2 u_1}{\partial X_1^2} + \nu\frac{\partial^2 u_2}{\partial X_1 \partial X_2} + \psi\left(\frac{\partial^2 u_1}{\partial X_2^2} + \frac{\partial^2 u_2}{\partial X_2 \partial X_1}\right) = 0 \text{ and } \frac{\partial^2 u_1}{\partial X_2^2} + \nu\frac{\partial^2 u_1}{\partial X_2 \partial X_1} + \psi\left(\frac{\partial^2 u_2}{\partial X_1^2} + \frac{\partial^2 u_1}{\partial X_1 \partial X_2}\right) = 0, \quad [S2]$$

where $\psi = (1 - \nu)/4$. The solution to Eq. S2 must satisfy the following boundary conditions: $u_1 = u_2 = 0$ where the membrane is in contact with the substrate, $u_1 = 0$ and $u_2 = u_0$ at the membrane edges, $\sigma_{22} = \Delta P_o$ along the top of the membrane, and $\boldsymbol{\sigma}\cdot\mathbf{n} = 0$ everywhere else, where $\mathbf{n}$ is the surface normal. The resulting boundary value problem is solved with the method of finite elements using the *pdenonlin* function in MATLAB (R2015a; Mathworks, Inc.).

S2. Modeling Adhesion of a Soft Membrane on Spherical Geometries

The FAM on the rigid system making contact with a spherical curved substrate is shown in Fig. S7. Additional boundary conditions and equations are employed to consider the mechanics of membrane adhesion on spherical substrates under a pressure differential. Initial boundary conditions for the vertical position of the system (z_0) and the contact radius (r_i) will be different depending on the size of the FAM with respect to the curved surfaces (Fig. S8). In the case that the spherical surface is larger than the adhesive membrane ($r_b \geq R_0$; Fig. S7b), the FAM achieves full contact prior to retraction, such that

$$z_0 = -r_b + \sqrt{r_b^2 - R_0^2} \text{ and } r_i = r_e. \quad [S3]$$

It should be noted that the position z is defined with respect to the origin and can be either positive or negative depending on the initial vertical position of the adhesion system (z_0) and retraction distance (z_r). Due to manufacturing imperfection and misalignment, the FAM on the rigid system could not often make full contact even on a flat substrate (Fig. S7d). We estimated from the experiments that approximately 700 μm from the edge of the FAM cannot make contact in average, which provides the maximum effective contact radius (r_e) to be 7.3 mm.

In the case when the spherical surface is smaller than the maximum effective contact radius ($r_b < r_e$; Fig. S7a), the FAM is assumed to be brought down to the center of the spherical substrate. The FAM wraps around the substrate, making conformal contact with the initial position and contact radius such that

$$z_0 = -r_b \text{ and } r_i = \frac{{r_b}^2}{R_0}. \quad [S4]$$

In experiments, the FAM could not be fully brought down to the center of the ball, as tensile stress may break the FAM during the preloading process. Instead, the system is brought down in contact until the preload reaches the predetermined value, which is in a range from 0.5 to 1.0 N. If the radius of a spherical substrate is in between the size of FAM and the effective maximum contact radius ($r_e \leq r_b < R_0$), the initial boundary conditions are

$$z_0 = -r_b \text{ and } r_i = r_e. \quad [S5]$$

During retraction, the FAM stretches due to adhesion, causing a volume change inside of the chamber (Fig. S7e). A volume in the shape of truncated cone deformation (V_t) subtracted with a volume of the spherical surface covered by the FAM in contact (V_c) increases the total volume (V) enclosed by the FAM in addition to the initial volume of the rigid adhesion system (V_0) as

$$V = V_0 - V_c + V_t. \quad [S6]$$

The initial volume (V_0) is the sum of the volume inside of the chamber, tubing, and syringe pump, which is approximately 7.2 mL. The volume inside of the truncated cone as well as the volume inside of the spherical cap covered by the FAM are

$$V_c = \frac{\pi h}{6}(3r^2+h^2) \text{ and } V_t = \frac{\pi}{3}(z+h)\left({R_0}^2+r^2+R_0 r\right), \quad [S7]$$

respectively, where $h = r_b - \sqrt{{r_b}^2 - r^2}$ is the vertical distance between the system and the top of the spherical surface.

The total potential energy (Π) of the FAM is calculated as a sum of elastic energy in a reference volume of detached area, adhesion energy of the membrane in contact, and work done by pressure can be modeled as

$$\Pi(r,z) = \pi\left({R_0}^2 - r^2\right)h_0 W_o(r,z) - \pi r^2 \omega_{\text{ad}} + U_p, \quad [S8]$$

where h_0 is the natural thickness of the FAM and ω_{ad} is the effective work of adhesion. The effective work of adhesion is the total energy required to separate two contact interfaces, which is used for estimating the resistance to interfacial peeling. Assuming that the FAM can be modeled as a Neo-Hookean solid, the strain energy density function W_o can be described as

$$W_0(r,z) = \frac{E_m}{6}\left({\lambda_\rho}^2 + {\lambda_\varphi}^2 + {\lambda_t}^2 - 3\right), \quad [S9]$$

The work done by air pressure (U_p) is

$$U_p = P_{atm}(V - V_0) - (P_{atm} + \Delta P_o)V_0 \ln\left(\frac{V}{V_0}\right). \quad [S10]$$

The critical contact radius (r_c) at a given value of vertical displacement of the system (z^*) can be calculated as the solution of the following equation for static equilibrium.

$$\left[\frac{\partial \Pi(r,z)}{\partial r}\right]_{z=z^*} = 0. \quad [S11]$$

By knowing the critical contact radius for different values of the vertical displacement which ranges from zero retraction distance (z_r) until the FAM is pulled off, the reaction force (F_r) can be calculated by taking the first partial derivative of the total potential energy ($\hat{\Pi}$) with respect to the given vertical displacement (z^*) and substituting the contact radius (r) with the critical contact radius (r_c) as

$$F_r(z^*) = \left[\frac{\partial \hat{\Pi}(z)}{\partial z}\right]_{z=z^*} = \frac{\partial \Pi(r_c, z^*)}{\partial z}. \quad \text{[S12]}$$

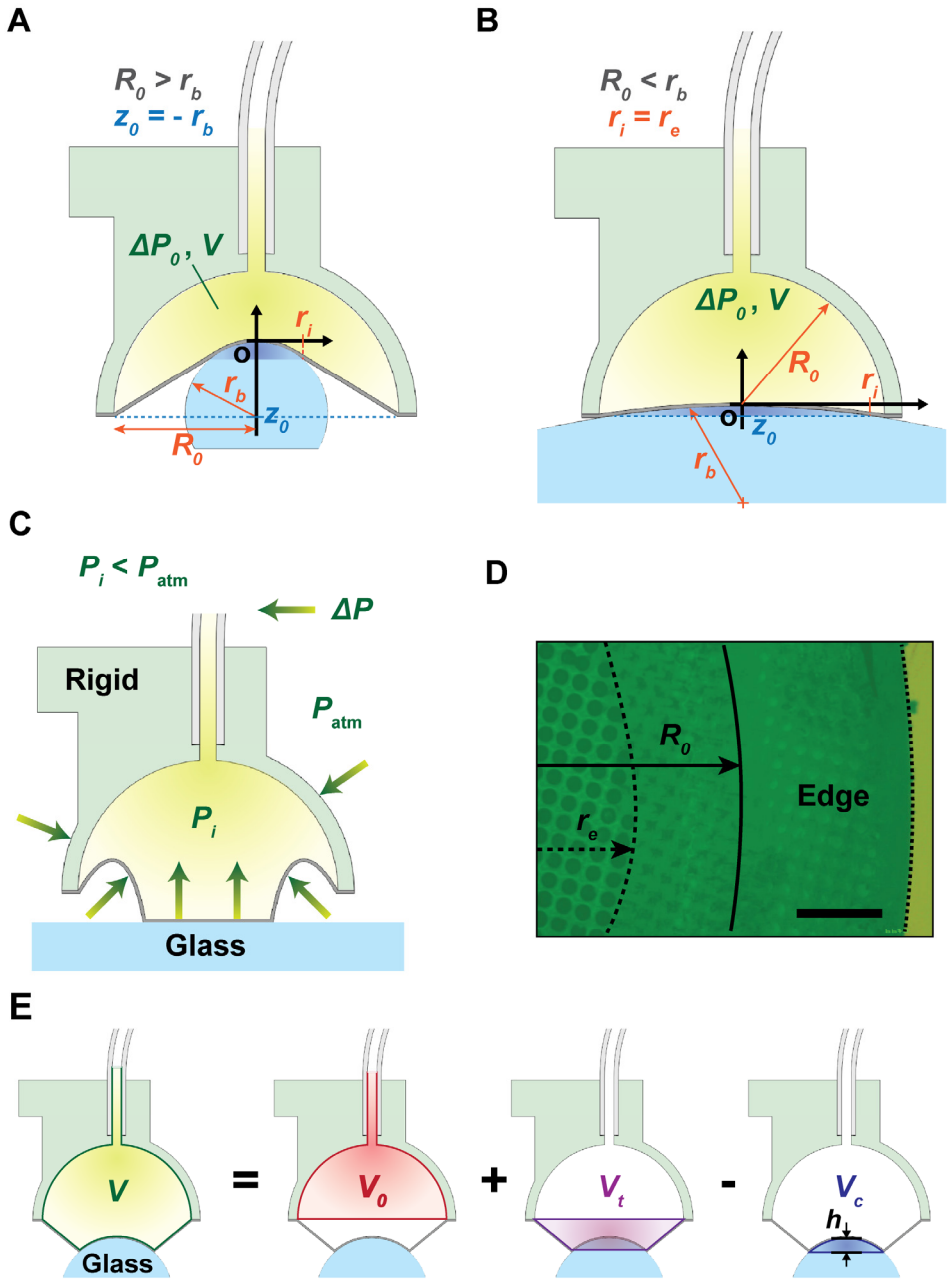

Fig. S7 Schematics of the analytical model for the rigid adhesion system with different boundary conditions. (A) A schematic of the rigid adhesion system in contact bigger than a spherical substrate. (B) A schematic of the contacting rigid adhesion system with a diameter that is smaller than that of the spherical substrate. (C) A schematic of the rigid adhesion system being delaminated from a flat glass substrate under a negative pressure differential (ΔP). Green arrows show the forces caused by the pressure differential acting on surface of the adhesion

system, which can pull the FAM into the rigid chamber and cause delamination of the membrane. (D) An inverted optical microscope image of the FAM on the rigid adhesion system in contact with a flat glass substrate, visualizing the contact interface. Dark areas indicate microfibers on the FAM in contact. The scale bar is 500 μm. (E) A schematic of the total volume (V) as a sum of the initial volume (V_0) and the additional volume created by the truncated-cone shaped deformation of the FAM (V_t), subtracted by the volume of the spherical substrate covered by the FAM (V_c). h is the height of the spherical cap (V_c).

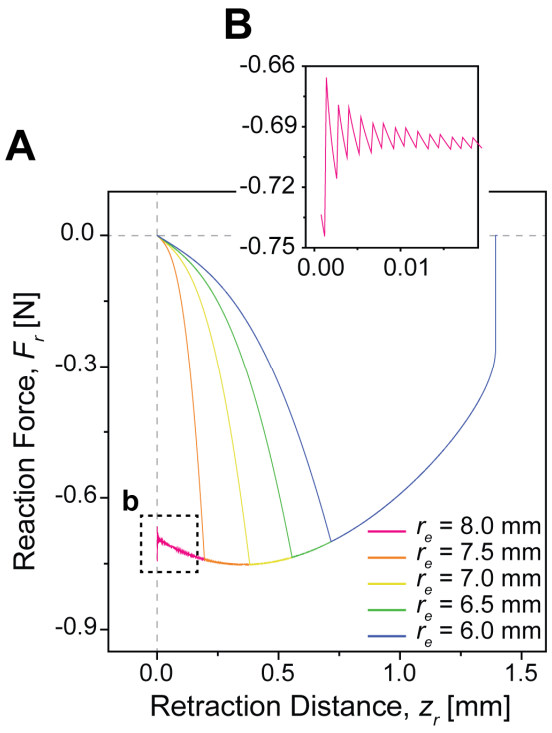

Fig. S8 (A) Calculated reaction force (F_r) profiles on a flat glass surface with respect to retraction distance (z_r), depending on effective contact radius (r_e). Here, the difference in the effective contact radius represents the difference in the initial contact area. (B) A magnified view for the reaction force profile in the beginning of retraction when r_e = 8.0 mm. Small numerical instabilities can be observed in the beginning of retraction when $r_e = R_0$. The first

derivatives of the total potential energy (Π) with respect to vertical displacement (z) and contact radius (r) are numerically obtained using the forward ($r_e = R_0$), centered ($0 < r_e < R_0$), and backward ($r_e = 0$) difference approximations. Here, the vertical displacement and contact radius are discretized in 20,001 and 50,001 elements, respectively.

S3. Adhesion characterization of both rigid and soft adhesion systems

Tables S1 and S2 show detailed information on a number of characterization results in adhesion of the rigid and soft adhesion systems, respectively. As mentioned in the experimental procedures, the air pressure inside of the adhesion systems is modulated by the volume change in the syringe connected to the chamber. The maximum pull-off force ($\underline{F_{\text{off}|\text{max}}}$) is the highest value on a given geometry on different initial pressures, while the minimum pull-off force ($F_{\text{off}|\text{min}}$) is the lowest pull-off force among measurements. The contact area (A_c) of the soft system is visually evaluated from the top-side through the transparent chamber. The contact area of the rigid system on non-planar geometries could not be visualized neither from the top nor the side. Therefore, the contact area on large objects, such as 60 mm of d_b glass sphere and flat glass are assumed to have the full contact of 1.7 cm^2 with the effective contact radius r_e = 7.3 mm. Note that the adhesion efficiency (ε_{ad}) of the soft system on the rubber film is not available, since the adhesion stress (σ_{ad}) of the FAM we tested is only valid on the interface between the PDMS-made fiber and glass substrate.

Table S1 | Characterization results of the rigid adhesion system

Characterization Parameters	d_b 15 mm	d_b 30 mm	d_b 60 mm	Flat Glass
Contact Area, A_c [cm^2]	N/A	N/A	1.7	1.7
Highest initial Pressure, $\Delta P_o\|_{\mathrm{h}}$ [kPa]	2.0	2.7	1.6	1.6
Lowest initial Pressure, $\Delta P_o\|_{\mathrm{l}}$ [kPa]	-0.7	-4.1	-3.2	-2.9
Min. Pull-off Force, $F_{\mathrm{off}}\|_{\mathrm{Min.}}$ [N]	0.13	0.12	0.30	0.52
Max. Pull-off Force, $F_{\mathrm{off}}\|_{\mathrm{Max.}}$ [N]	0.15	0.62	0.88	1.12
Enhancing Ratio, $F_{\mathrm{off}}\|_{\mathrm{Max.}}$ / $F_{\mathrm{off}}\|_{\mathrm{Min.}}$	1.2	5.0	3.0	2.2
Min. Adhesion Stress, $\sigma_{\mathrm{ad}}\|_{\mathrm{Min.}}$ [kPa]	N/A	N/A	1.2	2.0
Max. Adhesion Stress, $\sigma_{\mathrm{ad}}\|_{\mathrm{Max.}}$ [kPa]	N/A	N/A	3.5	4.4
Min. Adhesion Efficiency, $\varepsilon_{\mathrm{ad}}\|_{\mathrm{Min.}}$ [%]	N/A	N/A	1.8	3.1
Max. Adhesion Efficiency, $\varepsilon_{\mathrm{ad}}\|_{\mathrm{Max.}}$ [%]	N/A	N/A	5.2	6.6

Table S2 | Characterization results of the soft adhesion system

Characterization Parameters	d_b 15 mm	d_b 30 mm	d_b 60 mm	Flat Glass	Rubber Film
Contact Area, A_c [cm^2]	0.6	1.5	2.5	2.5	2.5
Highest initial Pressure, $\Delta P_o\|_{\mathrm{h}}$ [kPa]	1.5	0.6	3.6	1.7	0.3
Lowest initial Pressure, $\Delta P_o\|_{\mathrm{l}}$ [kPa]	-51.0	-50.7	-52.1	-51.7	-50.9
Min. Pull-off Force, $F_{\mathrm{off}}\|_{\mathrm{Min.}}$ [N]	0.18	0.42	0.49	0.66	0.08
Max. Pull-off Force, $F_{\mathrm{off}}\|_{\mathrm{Max.}}$ [N]	1.18	2.70	2.91	3.61	0.61
Enhancing Ratio, $F_{\mathrm{off}}\|_{\mathrm{Max.}}$ / $F_{\mathrm{off}}\|_{\mathrm{Min.}}$	6.7	6.4	6.0	5.4	7.2
Min. Adhesion Stress, $\sigma_{\mathrm{ad}}\|_{\mathrm{Min.}}$ [kPa]	2.8	2.8	1.9	2.6	0.3
Max. Adhesion Stress, $\sigma_{\mathrm{ad}}\|_{\mathrm{Max.}}$ [kPa]	18.7	18.1	11.4	14.2	2.4
Min. Adhesion Efficiency, $\varepsilon_{\mathrm{ad}}\|_{\mathrm{Min.}}$ [%]	3.9	3.9	2.6	3.6	N/A
Max. Adhesion Efficiency, $\varepsilon_{\mathrm{ad}}\|_{\mathrm{Max.}}$ [%]	25.7	25.0	15.8	19.5	N/A

S4. Characterization of the work of adhesion and adhesion stress of the FAM

Experimental methods for estimation of effective work of adhesion (ω_{ad}) of the FAM and its adhesion stress (σ_{ad}) have been standardized in several previous works based on Johnson, Kendall and Roberts (JKR) theory (2). Profiles of the reaction force (F_r) for a microfiber array on the FAM for both rigid and soft systems are shown in Fig. S9 with respect to vertical displacement (z). In order to rule out deformation of the soft PDMS backing during the measurements, the FAM is place on a flat glass substrate and fixed. A 4 mm radius (R) spherical glass indenter is brought down in contact with the FAM at an approach speed of 100 $\mu m \cdot s^{-1}$. The origin of z is set on the surface of the FAM, and positive z causes compression while negative z causes tension. A 100 mN of preload (F_{pre}) is applied by putting the spherical indenter down to the FAM. Here, we have 30 s of relaxation time to minimize unpredictable viscoelastic behavior of the elastomeric microfibers, which causes a slight decrease in reaction force profile. The indenter is pulled up with 50 $\mu m \cdot s^{-1}$ of retraction speed, which is the same speed used for the experimental measurements. The pull-off force of the microfiber array is measured at five different positions on the FAM; top, center, bottom, left, and right. The work of adhesion of the microfiber array on the FAM can be evaluated by the following relation between the work of adhesion and pull-off force based on JKR theory,

$$\omega_{ad} = {}^{2F_{off}}/_{3\pi R} \cdot \quad [S13]$$

Among the five measurements, three cases whose shape of contact is the most circular are selected in evaluating the projected contact area for the calculation in Eq. S13. The contact areas of those measurements are estimated from the still images at the instance of the fiber array pulling off from the surface using a conventional image processing software (ImageJ, NIH Image). Summary of the measurements in the pull-off force, along with the estimated work of adhesion and adhesion stress are shown in Tables S3 and S4.

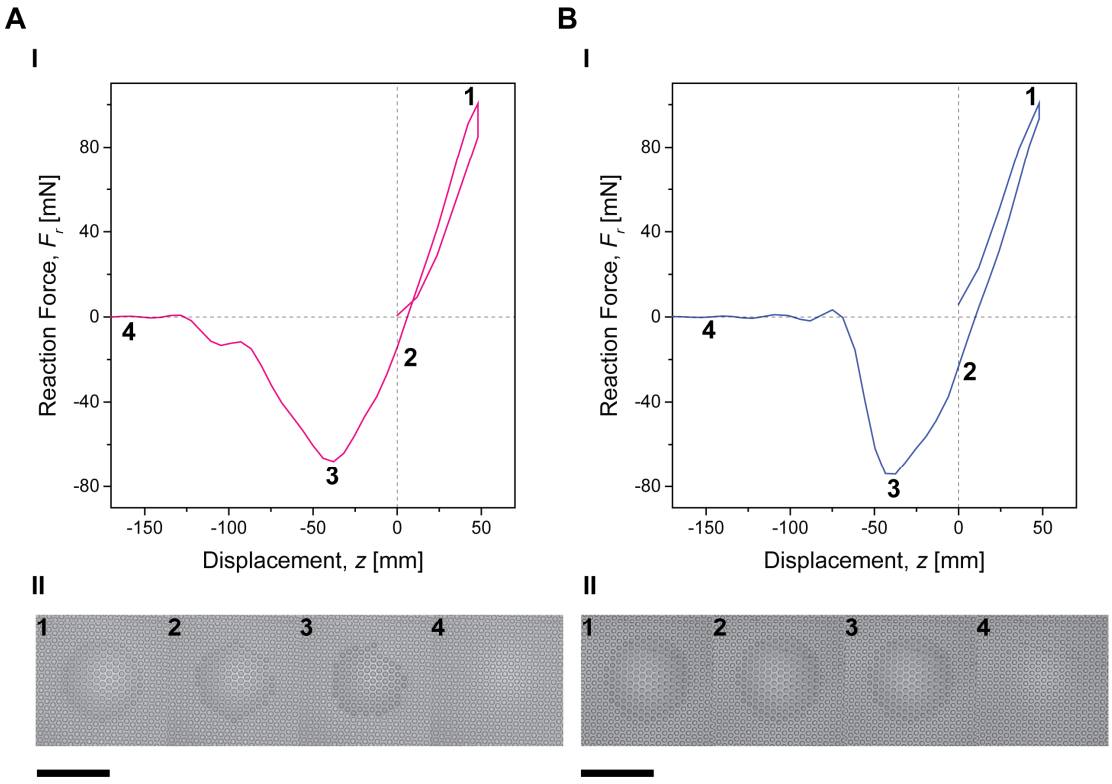

Fig. S9 Characterization of the effective work of adhesion (ω_{ad}) and adhesion stress (σ_{ad}) of the FAM for rigid and soft adhesion systems. (A) A reaction force (F_r) profile of the FAM for the soft system (I), in accordance with microscopic images on the interface (II). (B) A reaction force (F_r) profile of the FAM for the rigid system (I), in accordance with microscopic images on the interface (II). 1: preloading, 2: retracting, 3: exerting pull-off force, 4: detached. Scale bars indicate 1 mm.

Table S3 | Summary of F_{off}, ω_{ad} and σ_{ad} of the FAM for the rigid adhesion system

Position	Pull-off force, F_{off} [mN]	Projected Contact Area, A_{pc} [mm^2]
Top	66.3	
Center	82.1	
Bottom	80.6	0.78
Left	82.4	0.78
Right	78.8	0.76
AVG.	78.0	0.77
Work of Adhesion, ω_{ad} [J·m^{-2}]		4.1
Adhesion Stress, σ_{ad} [kPa]		100.8

Table S4 | Summary of F_{off}, ω_{ad} and σ_{ad} of the FAM for the soft adhesion system

Position	Pull-off force, F_{off} [mN]	Projected Contact Area, A_{pc} [mm^2]
Top	105.8	
Center	41.6	0.84
Bottom	55.1	
Left	68.0	0.87
Right	38.3	0.86
AVG.	61.8	0.86
Work of Adhesion, ω_{ad} [J·m^{-2}]		3.3
Adhesion Stress, σ_{ad} [kPa]		72.5

S5. Characterization of adhesion stress of a single fiber and small area of microfiber arrays on the FAM for the soft adhesion system

Estimation of adhesion stress of a single fiber ($\sigma_{ad|sf}$) and small area of microfiber arrays ($\sigma_{ad|3f}$) follow the experimental procedure for the FAM. Three samples (SPL) are taken from different areas of the FAM of the soft system. Each sample has three microfibers and is attached to a flat glass slide to measure the adhesion as shown in Fig. S10b. The 4 mm radius glass indenter is large enough for the three microfibers to make full contact and detach at the same time. The pull-off force of the three microfibers (F_{off}) is divided by the number of fibers and estimated as the pull-off force of a single fiber ($F_{off|sf}$). Each sample is measured 5x with 1 mN of preload (F_{re}).

Real contact areas of three microfibers (A_{rc}) on each sample are measured using the 3D confocal laser microscope as shown in Fig. S10a, and the real contact area of a single fiber ($A_{rc|sf}$) is estimated by dividing the measured area with the number of fibers. Projected contact areas of the three microfibers (A_{pc}) are estimated using the conventional image processing software (ImageJ, NIH Image), including spacing among the microfibers in addition to the real contact area (A_{rc}). Adhesion stresses of a single fiber and the three microfibers are calculated by dividing each adhesion with the estimated contact areas. Summary of the above measurements is shown in Table S5.

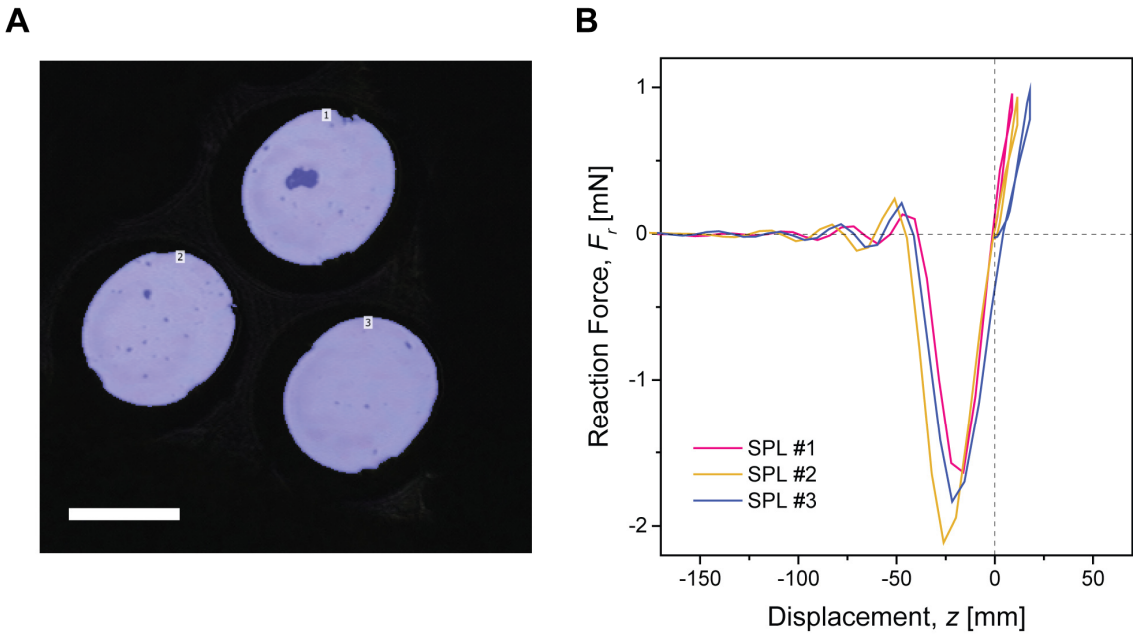

Fig. S10 Characterization of adhesion stress (σ_{ad}) of a single microfiber on the FAM for the soft adhesion system. (A) Visualization of the contact area of three microfibers for each samples using the confocal laser microscope. Scale bar = 100 μm. (B) Reaction force (F_r) profiles of three microfibers for each sample.

Table S5 | F_{off}, A_c and σ_{ad} of a single fiber and small area of microfiber array

Sample	Adhesion, F_{off} [mN]	Real Contact Area, A_{rc} [μm^2]	Projected Contact Area, A_{pc} [μm^2]
SPL #1	1.8	12787.0	20687.3
SPL #2	2.1	13451.3	20586.1
SPL #3	1.7	12552.0	21025.9
AVG.	1.9	12930.1	20766.4
Single Fiber Adhesion, $F_{off\|sf}$ [mN]			0.6
Single Fiber Real Contact Area, $A_{rc\|sf}$ [μm^2]			4310.0
Single Fiber Adhesion Stress, $\sigma_{ad\|sf}$ [kPa]			145.4
Three Fibers Adhesion Stress, $\sigma_{ad\|3f}$ [kPa]			90.5

References

1. Sadd MH (2014) *Elasticity: Theory, Applications, and Numerics* (Academic Press, Cambridge), 3rd Ed, pp 141-144.

2. Johnson KL, Kendall K, Roberts AD (1971) Surface Energy and the Contact of Elastic Solids. *Proceedings of the Royal Society A: Mathematical, Physical and Engineering Sciences* 324:301–313.